

Article

New Textural Indicators for Assessing Above-Ground Cotton Biomass Extracted from Optical Imagery Obtained via Unmanned Aerial Vehicle

Pengfei Chen ^{1,2,*} and Fangyong Wang ³

¹ State Key Laboratory of Resources and Environment Information System, Institute of Geographic Sciences and Natural Resources Research of Chinese Academy of Sciences, Beijing 100101, China

² Jiangsu Center for Collaborative Innovation in Geographical Information Resource Development and Application, Nanjing 210023, China

³ Cotton Institute, Xinjiang Academy of Agricultural and Reclamation Science, Shihezi 832000, China; fangyongwang425@163.com

* Correspondence: pengfeichen@igsrr.ac.cn

Received: 7 October 2020; Accepted: 17 December 2020; Published: 19 December 2020



Abstract: Although textural information can be used to estimate vegetation biomass, its use for estimating crop biomass is rare, and previous methods lacked a mechanistic explanation for the relationship to biomass. The objective of the present study was to develop mechanistic textural indices for estimating cotton biomass and solving saturation problems at medium and high biomass levels. A nitrogen (N) fertilization experiment was established, and unmanned aerial vehicle optical images and field measured biomass data were obtained during critical cotton growth stages. Based on these data, two textural indices, namely the normalized difference texture index combining contrast and the inverse difference moment of the green band (NBTI (CON, IDM)_g) and normalized difference texture index combining entropy and the inverse difference moment of the green band (NBTI (ENT, IDM)_g), were proposed by analyzing the mechanism of texture parameters for biomass prediction and the law of texture parameters changing with biomass. These indices were compared with spectral indices commonly used for biomass estimation using independent validation data, such as the normalized difference vegetation index (NDVI). The results showed that the proposed textural indices performed better than the spectral indices with no saturation problems occurring. The combination of spectral and textural indices using a stepwise regression method performed better for biomass estimation than using only spectral or textural indices. This method has considerable potential for improving the accuracy of biomass estimations for the subsequent delineation of precise cotton management zones.

Keywords: textural index; biomass; cotton; unmanned aerial vehicle; optical image

1. Introduction

Estimations of aboveground biomass act as an important indicator of crop vigor [1]. This indicator can be used to conduct crop yield forecasts [2], delineate management zones, and determine areas that require higher or lower amounts of fertilizer and herbicide (thereby increasing the income of farmers and reducing environmental pollution) [3]. For precision farming, these estimations must be made in a non-destructive manner, such that many studies have documented the use of remote sensing technology as an ideal tool for use in obtaining such information [4–6]. For example, to monitor crop biomass, studies have been conducted using spectral data measured from a satellite [7], manned aerial plane [8], and ground-based platform (comprising a tower and tractor) [9]. However, each platform has distinct advantages and disadvantages. Precision farming requires low-cost data at high spatial and temporal resolution at the field scale to support the timely implementation of

farmland management measures. The above traditional remote sensing platforms are unable to satisfy all requirements. For example, most data from satellites cannot have both high temporal and high spatial resolution; data from manned planes are expensive to acquire, and data from ground sensors are limited in spatial scope. Thus, new data acquisition platforms must be developed to support the acquisition of relevant data.

Unmanned aerial vehicles (UAVs) have attracted considerable scientific and public attention in recent years as they can take off at any time and are easily manipulated. When mounted with sensors, they can be used to acquire high spatial and temporal resolution images at a low cost [10]. UAVs are particularly useful in field-scale applications and can thus be employed to compensate for the limitations of traditional platforms. Data obtained via UAVs have already been used to conduct crop biomass estimations. For example, Wang et al. [11] estimated the biomass of perennial ryegrass based on the normalized difference vegetation index (NDVI) calculated from UAV-acquired multispectral images, and Niu et al. [12] used Red-Green-Blue (RGB) imagery measured from a four-rotor UAV to calculate various spectral indices and developed a corn biomass prediction model using a multivariable linear regression method.

However, using only spectral information does not always yield suitable results. Several studies have found that saturation problems occur when the canopy is closed and the biomass condition is high [13]. For example, Hunt et al. [14] acquired RGB images over soybeans, alfalfa, and a corn field from a fixed-wing UAV, reporting that the normalized green–red difference index (NGRDI) was sensitive to changes in the biomass of crops prior to canopy closure but insensitive after canopy closure. In addition, based on RGB images measured from a UAV, Yue et al. [15] found that designing a wheat biomass prediction model using only spectral information tended to cause an underestimation of the biomass value at a high biomass condition.

Compared with traditional remote sensing platforms, images acquired from UAVs have a high overlap rate. Thus, the 3D structure of crop canopies can be reconstructed from UAV images [16], and crop surface models (CSMs) can be used to extract plant height information in the field [17]. The crop height information can be used to estimate biomass. Bendig et al. [18] used UAV-acquired RGB images to extract the height of a barley canopy and successfully predicted barley biomass based on the height data [18]. Using hyperspectral images measured from UAVs, Yue et al. [1] found that wheat height was a proxy for biomass and that adding height information to a wheat biomass estimation model improved performance compared with only using spectral information. Nevertheless, extracting plant height from CSMs requires a digital elevation model of the field, which is laborious and time-consuming to obtain [19].

UAVs fly at a low altitude, and the images acquired have an ultrahigh spatial resolution of 1 cm (or higher). Such high spatial resolution images contain both spectral and textural information. As well as spectral information, textural information can be used to estimate vegetation biomass. Several studies have shown that image textural information can be used to estimate forest biomass [20–22]. However, until recently, only a few studies had estimated crop biomass based on textural information. In this respect, Yue et al. [15] used RGB (red, green, and blue) images obtained from a UAV; they resampled the images to provide different resolutions; used the grey level co-occurrence matrix (GLCM) method to extract different textural parameters from the resampled images; and then used a multiple stepwise regression technique to design a biomass estimation model based on spectral indices, textural parameters, and a combination of spectral indices and textural parameters, respectively. The best wheat biomass prediction results were obtained from the combined use of image spectral indices and textural parameters. In addition, based on multispectral images collected using a rotor UAV, Zheng et al. [19] first used the GLCM method to calculate the texture-based parameters and then used normalized formulation as the NDVI to combine all possible textural parameters to develop textural indices. Finally, they used a multiple stepwise regression technique to establish a biomass estimation model based on spectral indices, textural indices, and a combination of spectral and textural indices. Their results showed that using a combination of image spectral and textural information provided the

best rice biomass prediction, where the model using textural indices performed better than the model using spectral indices.

These studies have shown that combining spectral and textural information can improve predictions of biomass, promoting the application of image textural information for crop biomass estimation. However, they did not provide an explanation of the mechanism underlying the parameter setting during textural parameter calculations. Furthermore, they only used statistical methods to select textural parameters for biomass prediction or combined all possible textural parameters using normalized formulation as the NDVI to design textural indices and then constructed the biomass estimation model using all combined textural indices without considering the processes by which the variable is linked to biomass. A mechanistic explanation of the connection between textural parameters (or indices) and biomass has not yet been clarified, which affects the stability of the designed biomass estimation model. Therefore, previous studies have not yet fully exploited the potential of estimating crop biomass based on textural features.

Cotton is the most important natural textile fiber crop grown globally [23] and is important to the social and economic development of many countries. The total seed cotton yield in China accounts for approximately 30% of global cotton production, and Xinjiang contributes about 60% of China's cotton [24]. In Xinjiang, growers usually supply more water and fertilizer in the fields to achieve optimal yields [25]. Excess fertilizer results in several problems, including soil nutrient imbalance, declining yield and quality, and reduced income. Thus, in this region, it is important to precisely manage cotton production based on remote sensing estimated biomass. For cotton biomass estimation, studies have used spectral data measured from satellites and ground-based platforms [26,27]. However, until recently, no study has estimated cotton biomass using spectral and textural information from images acquired by a UAV platform, which is important for precision farming.

Therefore, the objectives of this study were as follows: (i) to examine the possibility of estimating the biomass of cotton based on textural features within images obtained from a UAV; (ii) to design a meaningful textural index that can be used to estimate the biomass of cotton; and (iii) to develop a biomass estimation model using a combination of spectral and textural information.

2. Materials and Methods

2.1. Field Experiment Design

Xinjiang is an arid area in Northwestern China. Cotton production in the area mainly uses a mulch drip irrigation method. In 2018, a cotton N field experiment was conducted in an experimental field at the Xinjiang Academy of Agricultural Reclamation Science (85°59'34.8"E, 44°18'43.2"N) in Shihezi, Xinjiang province (Figure 1), where cultivar "Xinluzao 64" was grown at a planting density of 237,600 plant ha⁻¹. The experiment used five N application levels of 0, 120, 240, 360, and 480 kg N ha⁻¹ applied in water via drip irrigation, with the use of a randomized block design with three replications. The size of each zone was 13.68 × 6 m². Plastic mulch, composed of polyethylene, with a colorless and transparent characteristic and a thickness of 0.01 mm was used to maintain soil moisture and temperature. Table 1 lists the dates of N application and the corresponding amounts. The soil type was grey desert soil, and the amounts of organic matter, total-N, available-P, and available-K were 13.83 g kg⁻¹, 1.14 g kg⁻¹, 7.50 mg kg⁻¹, and 198.70 mg kg⁻¹, respectively. With the exception of the differences in the amount of N added, the management of all fields was identical in each experimental zone. It should be noted that tillage measures were not applied to the field during the entire growing season of cotton.

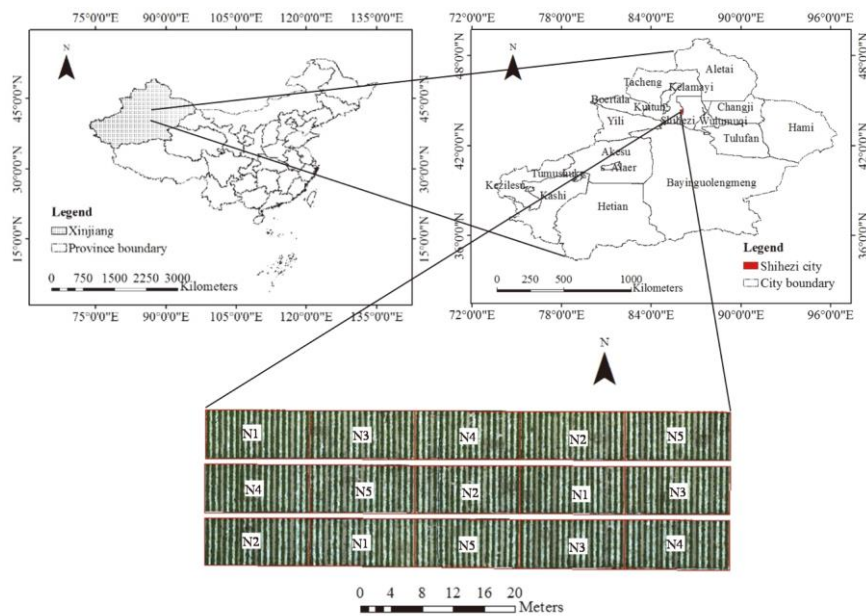


Figure 1. Location and layout of the cotton field experiment (N1: 0 kg N/ha; N2: 120 kg N/ha; N3: 240 kg N/ha; N4: 360 kg N/ha; and N5: 480 kg N/ha).

Table 1. Amount of nitrogen (N) applied with date of application.

Item	Fertilizer Application (Month and Day)							
	June 24	July 02	July 10	July 18	July 26	Aug. 4	Aug. 14	Aug. 24
N application ratio (%) ¹	9.5	12.5	13.5	15.5	16.0	13.5	12.0	7.5

¹ Proportion of amount of N applied to the total amount applied in each plot.

2.2. Data Collection

Field campaigns were conducted to sample the cotton biomass and collect UAV images during the peak square (23 June), early flower (11 July), peak flower (19 July), and boll (3 August) growth stages of cotton.

2.2.1. UAV Data

This study used a multispectral sensor, known as “RedEdge-M” (MicaSense, WA, USA), which contains five bands centered at 475 (Blue), 560 (Green), 668 (Red), 717 (Red-edge), and 840 nm (Near infrared). RedEdge-M was mounted on a four-rotor drone, known as “3DR Solo” (Berkeley, CA, USA), and flown under clear and cloudless conditions at an altitude of 40 m. Both the forward and side overlapping of UAV images were set at 75%. A white panel image was obtained prior to UAV take off, which was used to convert image data from the digital number (DN) values to reflection values during subsequent processing. Figure 2 shows the UAV employed and one of the captured images. Pix 4D Ag (Pix4D, Lausanne, Switzerland) was used to mosaic the acquired UAV images and convert the image DN values to reflectance values [28]. In addition, GPS points with an error of 1 cm were field sampled using Trimble GEO7X handheld GPS device (Trimble, CA, USA) and the real-time kinematic service provided by Qianxun (Shanghai, China) to geo-rectify the mosaicked images.

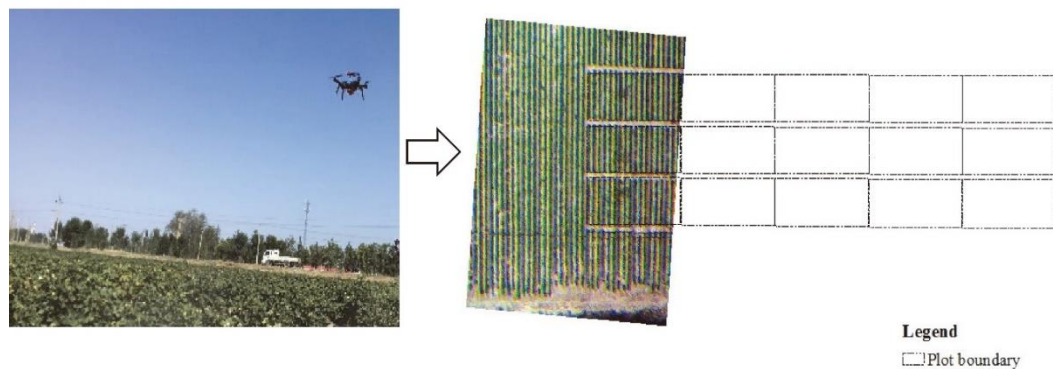


Figure 2. Unmanned aerial vehicle platform with one acquired image.

2.2.2. Field Data

Field measurements were conducted to measure the biomass immediately after the UAV images acquisition. Biomass data were obtained using a destructive sampling method in this study. A representative site in each plot was selected; three cotton plants were then sampled and taken to the laboratory, where the leaves, stems, and bolls were removed from the plants and then dried in an oven at 80 °C until a constant weight was attained. The biomass values for each plot were calculated by dividing the total weight of the stems, leaves, and bolls by the area of the sampled cotton in the corresponding sampling site.

2.3. Data Analysis Method

2.3.1. Design of the Candidate Textural Index for Estimating Cotton Biomass

Several methods are currently employed to extract textural parameters from images. Of these, the grey level co-occurrence matrix (GLCM) method proposed by Haralick [29] is the most commonly used. This method is easy to calculate and has been documented as performing well for vegetation biomass estimation [15,19]. Thus, this method was used in the present study.

A GLCM is first made from the analyzed image, followed by the calculation of the textural parameters from the GLCM. Several parameters must be set prior to developing the GLCM, which include the calculation window size, minimum and maximum gray values, the searching direction, and the number of gray levels. A fixed strategy for setting these parameters is thus required to ensure the application of the designed model, which has not been discussed in previous studies.

In this study, the window size, minimum and maximum gray values, the searching direction, and the number of gray levels were selected as follows. (1) For the window size, a larger observation window indicates that it is easier to detect the consistency of a target area, whereas a smaller observation window enables easier detection of the boundaries of different targets. We determined the window size based on the following premises: image classification was not required in this study, as our aim was to estimate the biomass in a precise management zone; therefore, the target was already known, and our aim was to only determine the biomass value. The field had been previously divided into different management zones, such that we wanted to estimate the crop biomass and ultimately develop precise management strategies. Based on the texture of an image, the internal mechanism for estimating the biomass of a target is related to changes in the pixel values of the image. Both soil and plant pixels exist in high resolution imagery, where their proportions change with crop growth. Due to the different soil and plant spectra, crop biomass can be estimated using the textural parameters of an image. Therefore, the window size was set to be identical to the size of the management plots used in this study. (2) Due to the different lighting conditions during UAV flight for each field campaign, the fixed maximum and minimum gray values were unable to be used for the UAV images (i.e., that were acquired at different times) when calculating the GLCM. Therefore, in this study, prior to calculating the GLCM of each acquired image, the maximum and minimum values of each band for the

entire study area were calculated and subsequently used. (3) For the searching direction, four angles (0° , 45° , 90° , and 135°) were used in accordance with the method described in Haralick et al. [29]. (4) Finally, to select an appropriate grey level number, the relationship between the textural parameters and biomass was investigated together with the changes in the grey level number. GLCM-based textural parameters were used here in accordance with previous studies [15,19,29], whose formulae can be found in Haralick et al.: angular second moment (ASM), contrast (CON), correlation (COR), variance (VAR), inverse difference moment (IDM), and entropy (ENT). Figure 3 shows the correlation coefficients between the textural parameters and biomass under different grey level numbers (2–50), and, in accordance with these results, the grey level number in this study was set to 15 to maintain computing efficiency and accuracy.

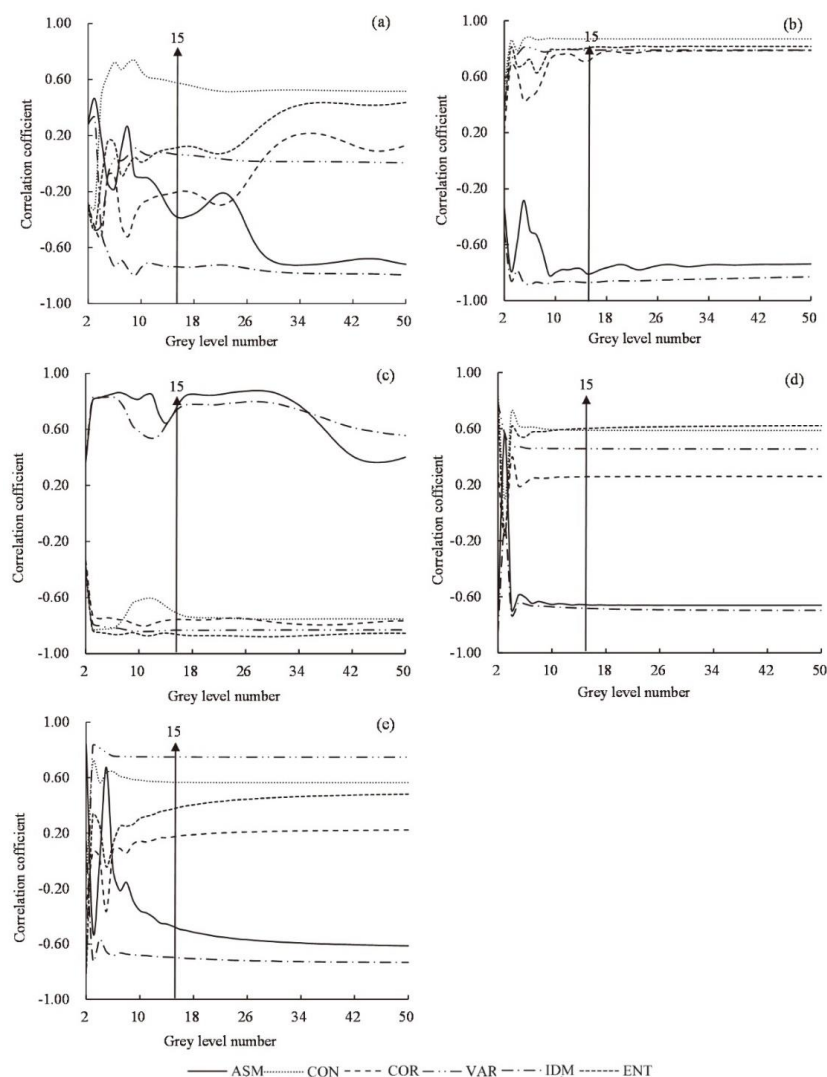


Figure 3. Correlation coefficients for textural parameters and biomass under different grey level numbers: (a) blue band, (b) green band, (c) red band, (d) red-edge band, and (e) near infrared band.

As shown in Figure 3, this study did not use textural parameters to compile a textural index for biomass prediction when the correlation between the textural parameters and biomass was unstable, as designing a textural index using these parameters may cause non-robust performance for biomass predictions. Therefore, only the following textural parameters were retained: CON and IDM from the blue band; all of the textural parameters from the green band; CON, COR, VAR, and ENT from the red band; ASM, CON, VAR, and IDM; and ENT from the red-edge and near infrared band. It should be

noted that VAR from the blue band and COR from the red-edge and near infrared bands were also discarded, as they had low relationships with the biomass ($p < 0.05$). Figure 3 also shows that, for each band, the trend between ASM and IDM and biomass was always opposite to the trend between CON, COR, VAR, and ENT and biomass. Therefore, the six textural parameters were divided into two groups, with ASM and IDM forming one group and the remaining textural parameters forming the second group. In consideration of the structure of the NDVI, it is possible to design an index for biomass estimation by combining one of the parameters from each of the two groups. Therefore, all possible combinations of the above selected textural parameters were used to design biomass indices for each band. The designed indices were named the “Biomass Normalized Textural Index (BNTI),” in which textural band abbreviations were employed with the band name as a suffix, which are listed in Table 2 and were considered as candidates for the selection of the best biomass textural indices (which are presented in Section 3.2). We note that, as both ASM and IDM from the red band were formerly discarded, a textural index in the red band was not constructed.

Table 2. Candidate textural indices for biomass estimation designed in this study.

Index	Formula
NBTI(CON, IDM) _b	$(CON_b - IDM_b)/(CON_b + IDM_b)$
NBTI(CON, ASM) _g	$(CON_g - ASM_g)/(CON_g + ASM_g)$
NBTI(CON, IDM) _g	$(CON_g - IDM_g)/(CON_g + IDM_g)$
NBTI(COR, ASM) _g	$(COR_g - ASM_g)/(CON_g + ASM_g)$
NBTI(COR, IDM) _g	$(COR_g - IDM_g)/(CON_g + IDM_g)$
NBTI(VAR, ASM) _g	$(VAR_g - ASM_g)/(CON_g + ASM_g)$
NBTI(VAR, IDM) _g	$(VAR_g - IDM_g)/(CON_g + IDM_g)$
NBTI(ENT, ASM) _g	$(ENT_g - ASM_g)/(CON_g + ASM_g)$
NBTI(ENT, IDM) _g	$(ENT_g - IDM_g)/(CON_g + IDM_g)$
NBTI(CON, ASM) _{re}	$(CON_{re} - ASM_{re})/(CON_{re} + ASM_{re})$
NBTI(CON, IDM) _{re}	$(CON_{re} - IDM_{re})/(CON_{re} + IDM_{re})$
NBTI(COR, ASM) _{re}	$(COR_{re} - ASM_{re})/(CON_{re} + ASM_{re})$
NBTI(COR, IDM) _{re}	$(COR_{re} - IDM_{re})/(CON_{re} + IDM_{re})$
NBTI(VAR, ASM) _{re}	$(VAR_{re} - ASM_{re})/(CON_{re} + ASM_{re})$
NBTI(VAR, IDM) _{re}	$(VAR_{re} - IDM_{re})/(CON_{re} + IDM_{re})$
NBTI(ENT, ASM) _{re}	$(ENT_{re} - ASM_{re})/(CON_{re} + ASM_{re})$
NBTI(ENT, IDM) _{re}	$(ENT_{re} - IDM_{re})/(CON_{re} + IDM_{re})$
NBTI(CON, ASM) _{nir}	$(CON_{nir} - ASM_{nir})/(CON_{nir} + ASM_{nir})$
NBTI(CON, IDM) _{nir}	$(CON_{nir} - IDM_{nir})/(CON_{nir} + IDM_{nir})$
NBTI(COR, ASM) _{nir}	$(COR_{nir} - ASM_{nir})/(CON_{nir} + ASM_{nir})$
NBTI(COR, IDM) _{nir}	$(COR_{nir} - IDM_{nir})/(CON_{nir} + IDM_{nir})$
NBTI(VAR, ASM) _{nir}	$(VAR_{nir} - ASM_{nir})/(CON_{nir} + ASM_{nir})$
NBTI(VAR, IDM) _{nir}	$(VAR_{nir} - IDM_{nir})/(CON_{nir} + IDM_{nir})$
NBTI(ENT, ASM) _{nir}	$(ENT_{nir} - ASM_{nir})/(CON_{nir} + ASM_{nir})$
NBTI(ENT, IDM) _{nir}	$(ENT_{nir} - IDM_{nir})/(CON_{nir} + IDM_{nir})$

g represents green band, re represents red-edge band, and nir represents near infrared band.

2.3.2. Biomass Prediction Model Design

The following procedures were used to design the biomass prediction model. (1) Commonly used spectral indices with potential for biomass prediction were selected (Table 3) and used to develop the biomass prediction model. The best spectral indices for cotton biomass estimation were then selected using data from the present study. When designing the model, linear, logarithmic, exponential, and power models were employed, and the best results were retained. The commonly mentioned saturation problem was then investigated with respect to using the selected spectral indices. (2) With the aim of selecting the best biomass textural indices, candidate textural indices were used to develop a biomass prediction model. Again, when designing the model, linear, logarithmic, exponential, and power models were also employed, and the best results were retained. The saturation problem with

respect to the selected textural indices was also investigated. Based on two previous studies [15,19] on crop biomass estimation using textural information from images, Zheng et al. [19] designed textural indices. The best of these textural indices, named the normalized difference texture index combining the mean of the near infrared band and green band (NDTI (MEA_{nir} , MEA_g)), was used in the present study to compare with the selected best textural index proposed herein. For calculating the two textural parameters (MEA_{nir} and MEA_g) in (NDTI (MEA_{nir} , MEA_g)), we completely followed the methods of Zheng et al. [20]. This involved using a window size of 3 pixels \times 3 pixels and calculating the mean value according to their formula. Then, MEA_{nir} and MEA_g were combined using normalized formulation as the NDVI to make NDTI (MEA_{nir} and MEA_g) according to Zheng et al. [19]. (3) A stepwise multiple regression method was used to develop the biomass estimation model based on selected spectral indices, textural indices, and both the spectral and textural indices. All of the developed models were then compared. As the relationship between the index and biomass may be non-linear, both Equations (1) and (2) were used to construct the model. Using Equations (1) and (2) to combine different indices, all possible situations were considered with respect to an index having a linear, logarithmic, exponential, or power relationship with the biomass. The combination providing the best results was used, which is presented in the following section. Note that a total of 60 samples were collected during the cotton growth season. Two-thirds of these samples were randomly selected and used for the calibration, and the remaining third were used for validation. The calibration and validation datasets were the same for all designed models mentioned above. The coefficient of determination (R^2), root mean square error (RMSE), and mean absolute percentage error (MAPE) were used to evaluate model performance [30].

$$y = a_0 + a_1 f_1(x_1) + \dots + a_n f_n(x_n) \quad (1)$$

$$\log_e(y) = a_0 + a_1 f_1(x_1) + \dots + a_n f_n(x_n) \quad (2)$$

where y is biomass; a_0, \dots, a_n are coefficients; and f_1, \dots, f_n are transformation algorithms, including a logarithm transformation ($\log_e(x_i)$), and non-transformation (x_i), which can be different from each other. In this respect, f_1 represents transformation of the original variable and has two forms: one uses the original value of the variable while the other uses a logarithm to transform the value of the variable.

Table 3. Summary of the spectral indices employed in this study.

Index	Full Name	Formula	Developed by
NDVI	Normalized Difference Vegetation Index	$(R_{nir} - R_{red}) / (R_{nir} + R_{red})$	Rouse et al. [31]
GNDVI	Green-Normalized Difference Vegetation Index	$(R_{nir} - R_{green}) / (R_{nir} + R_{green})$	Gitelson et al. [32]
MSAVI	Modified Soil-Adjusted Vegetation Index	$(2R_{nir} + 1 - \sqrt{(2R_{nir} + 1)^2 - 8(R_{nir} - R_{red})}) / 2$	Qi et al. [33]
OSAVI	Optimized Soil-Adjusted Vegetation Index	$1.16(R_{nir} - R_{red}) / (R_{nir} + R_{red} + 0.16)$	Rondeaux et al. [34]
EVI	Enhanced Vegetation Index	$2.5(R_{nir} - R_{red}) / (R_{nir} + 6R_{red} - 7.5R_{blue} + 1)$	Huete et al. [35]
TVI	Triangular Vegetation Index	$0.5(120(R_{nir} - R_{green}) - 200(R_{red} - R_{green}))$	Broge et al. [36]
MTVI2	Modified Triangular Vegetation Index 2	$1.5(1.2(R_{nir} - R_{green}) - 2.5(R_{red} - R_{green})) / \sqrt{(2R_{nir} + 1)^2 - (6R_{nir} - 5\sqrt{R_{red}}) - 0.5}$	Habouance et al. [37]
RVI	Ratio Vegetation Index	R_{nir} / R_{red}	Pearson et al. [38]
NDRE	Normalized Difference Red Edge	$(R_{nir} - R_{red-edge}) / (R_{nir} + R_{red-edge})$	Fitzgerald et al. [39]

3. Results

3.1. Best Spectral Indices for Estimating Cotton Biomass

Table 4 lists the calibration and validation results for designing cotton biomass estimation models using each spectral index. The best results were obtained using triangular vegetation index (TVI) and normalized difference red (NDRE). In this respect, during model calibration, the regression equations for TVI and NDRE provided R^2 values of 0.88 and 0.86, $RMSE$ values of 1.47 and 1.55 $t\ ha^{-1}$, and $MAPE$ values of 19.43% and 22.16%, respectively. When the biomass prediction models were tested using the validation dataset, their performance did not change, with R^2 values of 0.86 and 0.85, $RMSE$ values of 0.99 and 1.02 $t\ ha^{-1}$, and $MAPE$ values of 15.85% and 17.24%, respectively. Compared with the other indices, NDVI and RVI provided the worst results. During model calibration, NDVI and RVI returned R^2 values of 0.80 and 0.84, $RMSE$ values of 1.85 and 1.67 $t\ ha^{-1}$, and $MAPE$ values of 26.27% and 21.99%, respectively. When the models were validated by the validation datasets, their performances declined considerably, with R^2 values of 0.63 for both, $RMSE$ values of 1.61 and 1.64 $t\ ha^{-1}$, and $MAPE$ values of 25.32% and 22.92%, respectively. The remaining spectral indices provided moderate results when used to make the biomass prediction model. During model calibration, the R^2 values of their regression equations were between 0.83 and 0.86, with $RMSE$ values between 1.57 and 1.72 $t\ ha^{-1}$ and $MAPE$ values between 21.30% and 24.16%. When these models were validated by the validation datasets, their performances declined, with R^2 values between 0.70 and 0.79, $RMSE$ values between 1.21 and 1.43 $t\ ha^{-1}$ and $MAPE$ values of 19.18% and 22.55%. In summary, the TVI and NDRE were considered to be the best spectral indices for estimating biomass. Figure 4 shows the calibration and validation results of using the TVI and NDRE indices to estimate the biomass, where it can be observed that both the TVI and NDRE became insensitive to biomass changes at medium to high biomass levels, thus indicating saturation problems. The NDVI, GNDVI, MSAVI, OSAVI, EVI, and MTVI2 also had saturation problems (results are not shown for clarity).

Table 4. Calibration and validation results for the cotton biomass estimation models designed using the spectral indices. During model calibration, linear, logarithm, exponential, and power models were used to design the model, with the best results shown here.

Spectral Index	Calibration			Validation		
	R^2	$RMSE$ ($t\ ha^{-1}$)	$MAPE$ (%)	R^2	$RMSE$ ($t\ ha^{-1}$)	$MAPE$ (%)
NDVI	0.80	1.85	26.27%	0.63	1.61	25.32%
GNDVI	0.83	1.70	24.16%	0.73	1.36	21.77%
MSAVI	0.84	1.68	23.04%	0.73	1.38	21.70%
OSAVI	0.83	1.72	24.04%	0.71	1.42	22.55%
EVI	0.86	1.57	21.30%	0.79	1.21	19.18%
TVI	0.88	1.47	19.43%	0.86	0.99	15.85%
MTVI2	0.83	1.70	23.17%	0.70	1.43	22.33%
RVI	0.84	1.67	21.99%	0.63	1.64	22.92%
NDRE	0.86	1.55	22.16%	0.85	1.02	17.24%

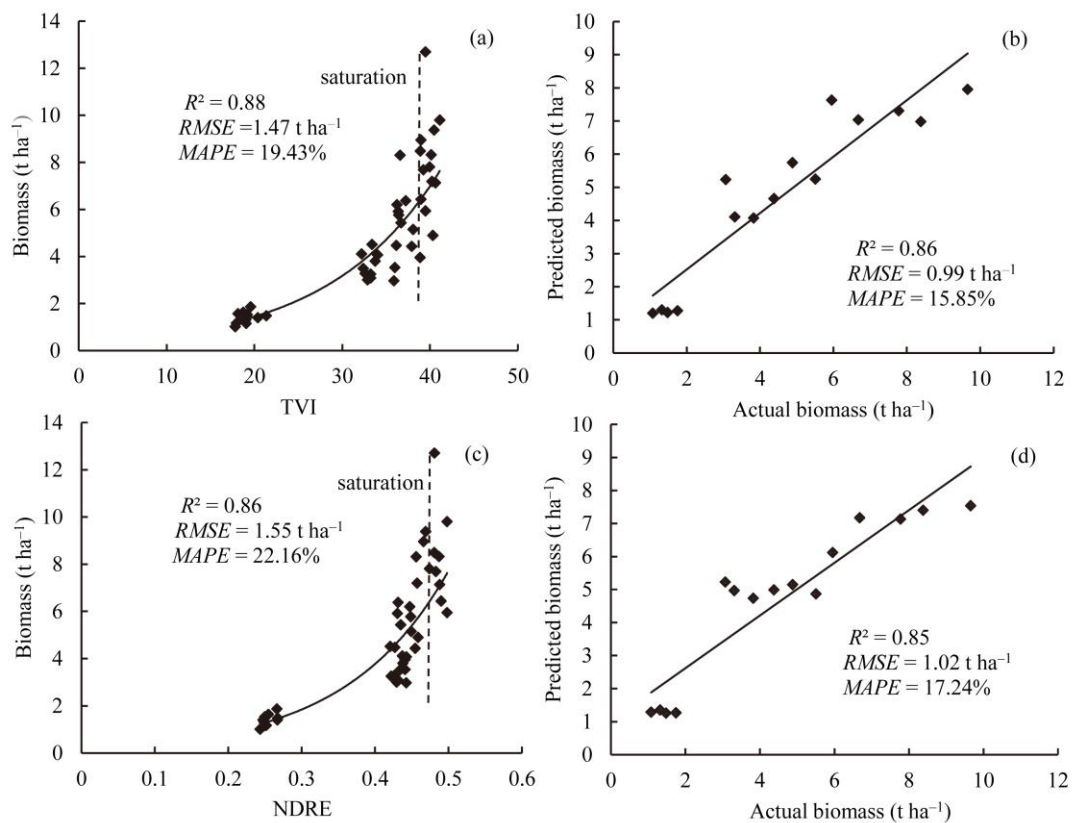


Figure 4. Results when using the triangular vegetation index (TVI) and normalized difference red (NDRE) indices to estimate the biomass. (a) Calibration results for TVI, (b) validation results for TVI, (c) calibration results for NDRE, and (d) validation results for NDRE.

3.2. Best Designed Textural Indices for Estimating Cotton Biomass

The calibration and validation results from using the designed candidate textural indices of the present study to estimate the biomass are shown in Table 5. The best results were achieved by NBTI (CON, IDM)_g and NBTI (ENT, IDM)_g. During model calibration, the R^2 values of the regression equations of NBTI (CON, IDM)_g and NBTI (ENT, IDM)_g were 0.84 and 0.81, respectively, with corresponding $RMSE$ values of 1.53 and 1.55 Mg ha⁻¹ and $MAPE$ values of 21.37% and 23.68%, respectively. The performance of the biomass prediction models did not change when tested using the validation dataset, with R^2 values of 0.88 and 0.87, $RMSE$ values of 1.04 and 0.97 Mg ha⁻¹, and $MAPE$ values of 18.46% and 17.67%, respectively. Compared with the other textural indices, NBTI (CON, ASM)_g, NBTI (COR, ASM)_g, NBTI (COR, IDM)_g, NBTI (VAR, ASM)_g, NBTI (VAR, IDM)_g, NBTI (ENT, ASM)_g, and NBTI (VAR, IDM)_{nir} provided moderate results. During model calibration, the R^2 values of their regression equations were between 0.60 and 0.79, with $RMSE$ values were between 1.54 and 1.90 t ha⁻¹ and $MAPE$ values were between 23.50% and 34.95%. When the models were validated using the validation datasets, the R^2 values of the designed models were between 0.66 and 0.90, with corresponding $RMSE$ values between 0.90 and 1.53 t ha⁻¹ and $MAPE$ values between 11.52% and 28.11%. The remaining spectral indices provided the worst results when used to construct the biomass prediction models. During model calibration, the R^2 values of their regression equations were between 0.32 and 0.72, with $RMSE$ values between 2.04 and 2.75 t ha⁻¹ and $MAPE$ values between 31.65% and 65.07%. When the models were validated using the validation datasets, their R^2 values were between 0.12 and 0.53, with $RMSE$ values between 1.77 and 2.70 t ha⁻¹ and $MAPE$ values between 28.14% and 59.19%. Therefore, NBTI (CON, IDM)_g and NBTI (ENT, IDM)_g were considered to be the best textural indices for use in estimating cotton biomass. Figure 5 show their calibration and validation results when estimating biomass, where it can be observed that both the NBTI (CON, IDM)_g and NBTI (ENT, IDM)_g

IDM)_g maintain sensitivity to changes in the biomass at medium to high biomass levels and thus do not have saturation problems.

The existing textural index for biomass estimation (NDTI(MEA_{nir}, MEA_g)) provided an R^2 value of 0.69, $RMSE$ value of 4.62 t ha⁻¹, and $MAPE$ value of 31.71% during calibration, and an R^2 value of 0.51, $RMSE$ value of 2.36 t ha⁻¹, and $MAPE$ value of 28.62% during validation. Thus, for cotton biomass estimation, NBTI (CON, IDM)_g and NBTI (ENT, IDM)_g performed far better than NDTI(MEA_{nir}, MEA_g).

Table 5. Calibration and validation results for the cotton biomass estimation models designed using textural indices. During model calibration, linear, logarithm, exponential, and power models were used to design model, with the best results shown here.

Spectral Index	Calibration			Validation		
	R^2	$RMSE$ (t ha ⁻¹)	$MAPE$ (%)	R^2	$RMSE$ (t ha ⁻¹)	$MAPE$ (%)
NBTI(CON, IDM) _b	0.32	2.30	65.07	0.52	1.85	59.19
NBTI(CON, ASM) _g	0.79	1.56	25.51	0.81	1.15	20.23
NBTI(CON, IDM) _g	0.84	1.53	21.37	0.88	1.04	18.46
NBTI(COR, ASM) _g	0.60	1.81	34.95	0.87	1.16	26.72
NBTI(COR, IDM) _g	0.61	1.83	34.45	0.87	1.05	23.71
NBTI(VAR, ASM) _g	0.74	1.58	26.11	0.90	0.94	16.11
NBTI(VAR, IDM) _g	0.79	1.54	23.50	0.89	0.90	11.52
NBTI(ENT, ASM) _g	0.73	1.66	28.35	0.82	1.12	22.51
NBTI(ENT, IDM) _g	0.81	1.55	23.68	0.87	0.97	17.67
NBTI(CON, ASM) _{re}	0.66	2.14	34.21	0.51	1.87	28.82
NBTI(CON, IDM) _{re}	0.72	2.04	31.65	0.53	1.77	30.02
NBTI(COR, ASM) _{re}	0.61	2.20	37.22	0.51	1.90	28.14
NBTI(COR, IDM) _{re}	0.64	2.24	34.79	0.43	2.01	29.75
NBTI(VAR, ASM) _{re}	0.66	2.19	34.17	0.48	1.93	28.62
NBTI(VAR, IDM) _{re}	0.65	2.31	34.39	0.38	2.10	30.10
NBTI(ENT, ASM) _{re}	0.66	2.18	34.45	0.47	1.93	30.18
NBTI(ENT, IDM) _{re}	0.68	2.20	32.12	0.40	2.05	32.95
NBTI(CON, ASM) _{nir}	0.58	2.37	38.70	0.33	2.25	35.08
NBTI(CON, IDM) _{nir}	0.66	2.09	34.87	0.48	1.83	34.18
NBTI(COR, ASM) _{nir}	0.35	2.74	48.43	0.13	2.67	40.13
NBTI(COR, IDM) _{nir}	0.37	2.75	47.53	0.13	2.65	39.44
NBTI(VAR, ASM) _{nir}	0.66	2.16	35.49	0.46	1.99	32.71
NBTI(VAR, IDM) _{nir}	0.76	1.90	29.05	0.66	1.53	28.11
NBTI(ENT, ASM) _{nir}	0.42	2.65	45.22	0.12	2.70	41.26
NBTI(ENT, IDM) _{nir}	0.58	2.44	37.81	0.24	2.41	36.11
NDTI(MEA _{nir} , MEA _g) [*]	0.69	4.62	31.71	0.51	2.36	28.62

^{*} designed by Zheng et al. [19].

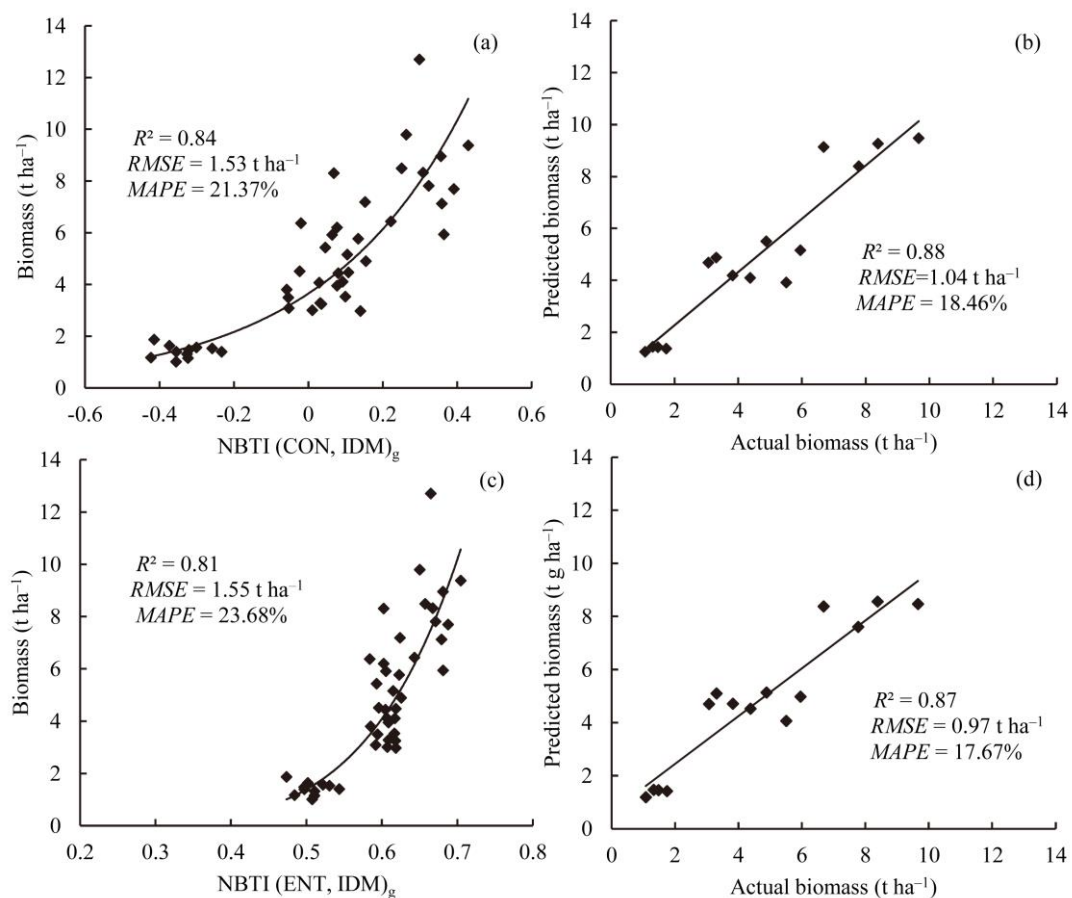


Figure 5. Results when using $NBTI (CON, IDM)_g$ and $NBTI (ENT, IDM)_g$ to estimate the biomass. (a) Calibration results for $NBTI (CON, IDM)_g$, (b) validation results for $NBTI (CON, IDM)_g$, (c) calibration results for $NBTI (ENT, IDM)_g$, and (d) validation results for $NBTI (ENT, IDM)_g$.

3.3. Results of Biomass Estimation Based on the Different Methods Used to Design Models

Based on the stepwise regression model proposed in this study and the calibration dataset, the best models used to estimate biomass (spectral indices, textural indices, and both spectral indices and textural indices) have R^2 values of 0.88, 0.84, and 0.89, respectively, which are described by Equations (3)–(5), respectively, as follows:

$$\log_e (\text{Biomass}) = -1.211 + 0.079TVI (R^2 = 0.88) \quad (3)$$

$$\log_e (\text{Biomass}) = 1.294 + 2.6040NBTI (CON, IDM)_g (R^2 = 0.84) \quad (4)$$

$$\log_e (\text{Biomass}) = -0.354 + 0.974 NBTI (CON, IDM)_g + 0.0520TVI (R^2 = 0.89) \quad (5)$$

Equations (3)–(5) can then be transformed into Equations (6)–(8) as follows:

$$\text{Biomass} = 0.2979 e^{0.0790TVI} \quad (6)$$

$$\text{Biomass} = 3.6474 e^{2.6040NBTI (CON, IDM)_g} \quad (7)$$

$$\text{Biomass} = 0.7019 e^{0.0520TVI+0.974NBTI (CON, IDM)_g} \quad (8)$$

Notably, only TVI was selected as a predictor for biomass estimation when using the spectral indices, whereas only $NBTI (CON, IDM)_g$ was selected as a predictor for biomass estimation when using the textural indices. Therefore, the relationships between the TVI and NDRE, and between the $NBTI (ENT, IDM)_g$ and $NBTI (CON, IDM)_g$, were investigated and are shown in Figure 6. The TVI had

a close relationship with NDRE (correlation coefficient value of 0.99) while NBTI (ENT, IDM)_g had a close relationship with NBTI (CON, IDM)_g (correlation coefficient of 0.99), which indicates that they contain substantial common information. This may be the reason why only one index was selected when developing the biomass estimation models using only spectral or textural indices. When tested by the validation dataset, models (6) and (7) provided R^2 values of 0.86 and 0.88 and corresponding $RMSE$ values of 0.99 and 1.04 t ha⁻¹ and $MAPE$ values of 15.85% and 18.46%, respectively, which are shown in Figures 4b and 5b, respectively. When using both the spectral and textural indices to estimate the biomass, a spectral index (TVI) and a textural index (NBTI (CON, IDM)_g) were selected to develop the stepwise regression model, with an $RMSE$ value of 1.33 t ha⁻¹ and $MAPE$ value of 17.51%. When the model was tested using the validation dataset, it performed better than the models constructed only with spectral or textural indices, yielding an R^2 value of 0.91, $RMSE$ value of 0.83 t ha⁻¹, and $MAPE$ value of 15.24% (Figure 7).

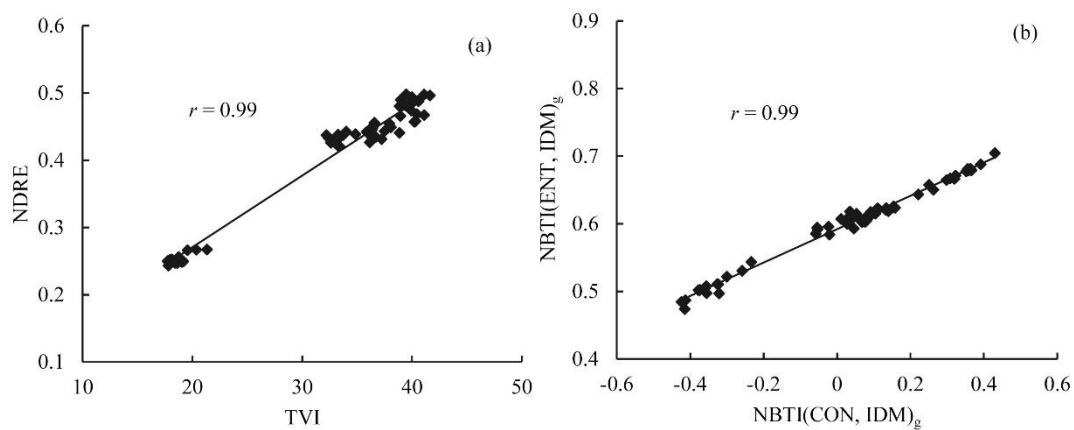


Figure 6. Relationship between (a) TVI and NDRE and (b) between NBTI (CON, IDM)_g and NBTI (ENT, IDM)_g.

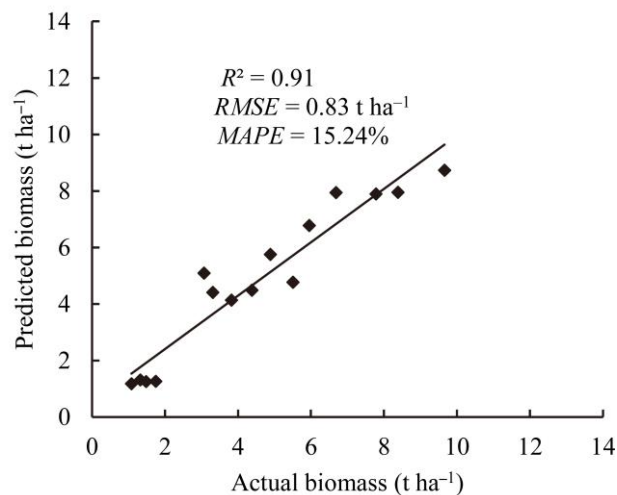


Figure 7. Validation results for the model developed by combining the spectral and textural information.

4. Discussion

4.1. Mechanism Explanation for Selected Textural Indices

In this study, NBTI (CON, IDM)_g and NBTI (ENT, IDM)_g were selected as the best textural indices. For the composition of NBTI (CON, IDM)_g and NBTI (ENT, IDM)_g, CON is a measure of the contrast or the amount of local variation present in an image [29], ENT is a measure of the complexity present in an image [3], and IDM is a measure of the local homogeneity present in an image [40]. Therefore,

as previously mentioned, changes in IDM are always opposite to those of CON and ENT. Figure 8 shows the relationship between the biomass- and GLCM-based textural parameters, where we observe that the correlation trends between the textural parameters and biomass differ between the red band and other bands. This occurs due to the following reasons. (i) Vegetation has strong absorption in the red band, which makes reflectance from pure vegetation pixels during different growth states similar to those of crop–soil mixed pixels. (ii) The cotton field soil was covered in mulch, which has an evidently higher reflectance value than vegetation in the visible bands, such that this difference is more pronounced in the red band than in green and blue bands. These two reasons makes it impossible to divide pure vegetation pixels during the different growth states and crop–soil mixed pixels into different grey levels (or it is only possible to divide them into a few adjacent grey levels) when the maximum and minimum reflectance values are used as maximum and minimum parameters and the grey level number is set to not a particularly high value during constructing the GLCMs. Therefore, when the growth of the cotton on the plant gradually began to cover most of the pixels in an image, CON and ENT had a negative relationship with biomass and IDM had a positive relationship with biomass in the red band (Figure 3c). In contrast, in the green, red-edge, and near infrared bands, pure vegetation pixels during different growth states and crop–soil mixed pixels can be divided into different grey levels. The soil pixels covered by plastic mulch, which has a more uniform reflectance value, began to disappear when the cotton started to grow. This caused CON and ENT to have a positive relationship with biomass and IDM to have a negative relationship with biomass in the green, red-edge, and near infrared bands (Figure 3b,d,e). For the blue band, although vegetation also has high absorption, there was not a substantial difference between the reflectance value of the soil pixels and that of the vegetation pixels. The trend between the GLCM-based parameters in the blue band and biomass varies with changes in the grey level number from a small to large number (Figure 3a). According to the above analysis, using a combination of CON_g , IDM_g , and ENT_g with an NDVI-like formula yields a positive correlation between NBTI (CON, IDM)_g and NBTI (ENT, IDM)_g and biomass (Figure 5), which can be used for biomass estimation.

4.2. Importance of Adding Textural Information When Estimating Biomass

As previously mentioned, saturation problems can occur when estimating crop biomass using only spectral information at high biomass conditions. With the development of remote sensing technology, an increasing number of high-resolution images are available for use, which has increased since the development and application of UAV remote sensing technology. High resolution images not only contain spectral information, but they are also rich in textural information. Several studies have suggested that the use of textural information to predict vegetation biomass provides good results [21,22]. Although quite a few studies have focused on crops [15,19], this may be a solution to solve saturation problems in field crop biomass estimations.

To estimate the winter wheat biomass, Yue et al. [15] obtained R^2 values between 0.59 and 0.78 and corresponding $RMSE$ values between 1.22 and 1.59 t ha⁻¹, respectively, based only on spectral information. When adding textural information, the model's performance was enhanced and an R^2 value of 0.89 and $RMSE$ value of 0.82 t ha⁻¹ was obtained. Zheng et al. [19] also estimated rice biomass, obtaining an R^2 value of 0.63 when using only spectral indices, but an R^2 value of 0.78 and $RMSE$ value of 1.84 t ha⁻¹ when employing both spectral and textural information. The above two previous studies reported that using a combination of textural and spectral information to estimate biomass performed better than using only spectral information. These findings were confirmed in the present study when cotton biomass was estimated. When using spectral information to predict biomass in this study, a saturation problem occurred when the cotton biomass was at a medium to high level. Note that the saturation problems of the spectral indices were also observed by Gitelson [32] and Chen et al. [41]. It was also found that the designed textural indices had a high relationship with biomass, such that when textural information was used to estimate biomass, there was no saturation problem. When the stepwise method was used to select the variables for biomass estimation based on

all spectral and textural indices, the selected variables were derived from both the spectral and textural indices. The model performed better when combining the selected variables to predict biomass than when only employing the spectral or textural indices. These results demonstrate that using both the spectral and textural information provides a superior estimation of biomass.

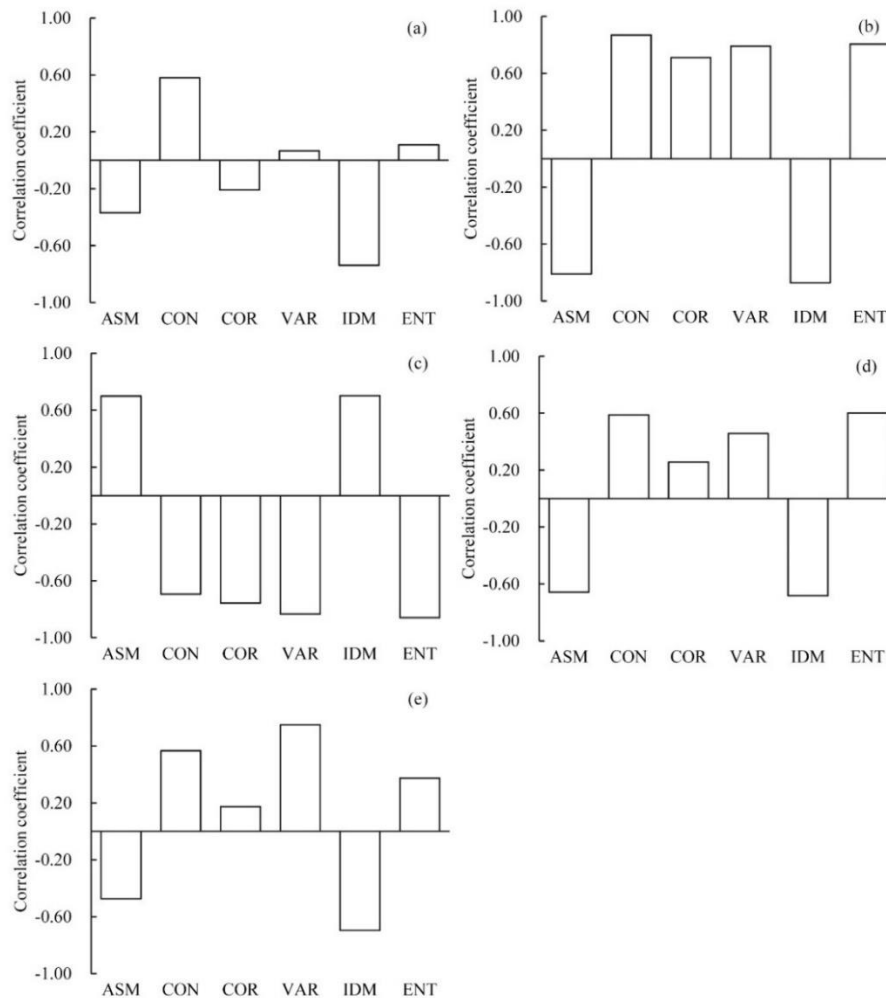


Figure 8. Relationships between the biomass and GLCM-based textural parameters calculated from the (a) blue band, (b) green band, (c) red band, (d) red-edge band, and (e) near infrared band. ASM: Angular Second Moment; CON: Contrast; COR: Correlation; VAR: Variance; IDM: Inverse Difference Moment; ENT: Entropy.

4.3. Previous Difficulties in Application of Textural Information and New Changes

Previous studies have long acknowledged that images contain textural information [29,42], where such information has been used to estimate forest biomass for a number of years [21,43]. However, using this information has not been considered a popular method for use in estimating vegetation biomass, particularly for crop biomass predictions. This has mainly been due to the lack of high resolution images, but also because there was no criterion for calculating textural parameters. For example, with respect to the GLCM method, numerous parameters must be set prior to using it to calculate textural information; such parameters affect the final textural parameter calculation results. Sarker and Nichol [21] found that setting the window size when calculating the GLCM influenced the forest biomass estimation results when using imagery from the Advanced Land Observation Satellite. Yue et al. [15] also found that the window size required special consideration when estimating winter wheat biomass using UAV images. In this study, in addition to the window size, we found that setting

the grey level number when calculating the GLCM influenced the relationship between the calculated textural parameters and the biomass (Figure 3). Therefore, standardizing the process used to calculate textural information is important to promote its application in biomass estimation. This study thus proposes a calculation process for use in estimating the cotton biomass based on textural information in precision agriculture with a zoning management strategy.

Yue et al. [15] used multiple stepwise regression methods to directly combine textural parameters from images at different resolutions to estimate wheat biomass without designing a textural index. Their methods had the following limitations: (i) criteria for parameter setting while calculating the GLCM were not provided; (ii) no mechanistic explanation was offered for the relationship of textural parameters selected using stepwise regression to biomass; (iii) for application, it is difficult to determine how many types of resolution images are suitable for estimating the biomass of different crops, and image resampling causes a loss of texture information; and (iv) compared to the texture index, textural parameters were more susceptible to influence from external factors such as lighting conditions during image acquisition. Compared with Yue et al. [15], Zheng et al. [19] used a normalized formulation as the NDVI to combine all possible textural parameters to develop textural indices and then selected the best index based on their database. However, they did not provide a mechanistic explanation of how the texture parameters constituting the best textural index were selected and how the textural index is related to biomass. This may lead to lower performance of the selected textural index for biomass estimation. Based on the data in the present study, Zheng et al.'s best textural index did not perform well for cotton biomass estimation. Therefore, compared with previous studies, the present study determined the criteria for parameter setting during each step of textural information extraction, and we propose textural indices together with a clear explanation of the involved mechanisms. This has the potential to provide, in practice, a more robust performance.

4.4. Application of Textural Indices

In this study, the window size was set to be identical to that of the management zone when calculating the GLCM-based textural parameters, as this is suitable for use in precision agriculture. However, the textural indices calculated based on this method can also be used for vegetation biomass estimation in other fields, as long as the spatial units are divided according to the desired scale in advance.

This study considered the characteristics of cotton fields when designing the textural indices. Cotton fields in China are mainly planted in arid and semi-arid areas in the western regions, with the adaptation of a mulch drip irrigation field management strategy. The reflectance of the plastic mulch is different from that of bare soil, such that it causes a different crop canopy spectrum effect. Therefore, the designed textural indices in this study are currently suitable for use in plastic mulched cotton fields or other crops that are mulched in the same manner, but their use with bare soil has yet to be verified. However, the design of textural indices presented in this study can be used as a reference for constructing relevant textural indices in other scenarios.

5. Conclusions

Cotton was grown with the addition of N at varying quantities and applied at different times. UAV images and field data were obtained during the critical cotton growth stages and, based on these data, this study designed new textural indices for estimating cotton biomass. These indices differ from those in previous research, as the criterion for setting each parameter used to calculate the GLCM-based textural parameters was clarified when designing the textural indices. The mechanism(s) for designing the textural indices was presented here to illustrate the robustness of the designed textural indices for biomass prediction and to serve as an example when constructing textural indices in other scenarios. The two textural indices, i.e., NBTI (CON, IDM)_g and NBTI (ENT, IDM)_g, recommended for use by this study were found to have a close relationship with the biomass, with the occurrence of no saturation problems at medium to high biomass levels. A stepwise regression method was used to develop

biomass prediction models based on the spectral indices, textural indices, and both the spectral and textural indices. It was found that the model designed by combining the spectral and textural indices performed better than the other two model types. However, the designed textural indices have only been tested in cotton fields with plastic mulch. For further study, a large database with different image data, crop species, years, and sites should be compiled and used to validate the designed textural indices and concept presented in this study. It was speculated that the method proposed in this study has great potential for improving the accuracy of cotton biomass predictions, and its application in other analogous fields.

Author Contributions: P.C. designed the experiment, performed the analysis and wrote the paper; F.W. help collected the field data and revised the paper. All authors have read and agreed to the published version of the manuscript.

Funding: This research was funded by the National Research and Development Plan of China, grant number 2016YFD0200603; the National Natural Science Foundation of China, grant number 41871344, 31560342; and the Strategic Priority Research Program of the Chinese Academy of Sciences, grant number XDA23100101.

Acknowledgments: The authors thank Jinran Liu and Zhitao Xu for their valuable assistance during the field campaign. We also thank for the four anonymous reviewers for their critical comments on the manuscript.

Conflicts of Interest: The authors declare no conflict of interest.

References

1. Yue, J.; Yang, G.; Li, C.; Li, Z.; Wang, Y.; Feng, H.; Xu, B. Estimation of winter wheat above-ground biomass using unmanned aerial vehicle-based snapshot hyperspectral sensor and crop height improved models. *Remote Sens.* **2017**, *9*, 708. [[CrossRef](#)]
2. Ghassemi-Golezani, K.; Tajbakhsh, Z. Relationship of plant biomass and grain filling with grain yield of maize cultivars. *Int. J. Agric.* **2012**, *4*, 1536–1539.
3. Barbieri, A.L.; de Arruda, G.F.; Rodrigues, F.A.; Bruno, O.M.; da Fontoura Costa, L. An entropy-based approach to automatic image segmentation of satellite images. *Phys. A* **2011**, *390*, 512–518. [[CrossRef](#)]
4. Hansen, P.M.; Schjoerring, J.K. Reflectance measurement of canopy biomass and nitrogen status in wheat crops using normalized difference vegetation indices and partial least squares regression. *Remote Sens. Environ.* **2003**, *86*, 542–553. [[CrossRef](#)]
5. Campos, I.; Gonzalez-Gomez, L.; Villodre, J.; Gonzalez-Piqueras, J.; Suyker, A.E.; Calera, A. Remote sensing-based crop biomass with water or light-driven crop growth models in wheat commercial fields. *Field Crops Res.* **2018**, *216*, 175–188. [[CrossRef](#)]
6. Liao, C.H.; Wang, J.F.; Dong, T.F.; Shang, J.L.; Liu, J.G.; Song, Y. Using spatio-temporal fusion of Landsat-8 and MODIS data to derive phenology, biomass and yield estimates for corn and soybean. *Sci. Total Environ.* **2019**, *650*, 1707–1721. [[CrossRef](#)]
7. Machwitz, M.; Giustarini, L.; Bossung, C.; Frantz, D.; Schlerf, M.; Lilienthal, H.; Wandera, L.; Matgen, P.; Hoffmann, L.; Udelhoven, T. Enhanced biomass prediction by assimilating satellite data into a crop growth model. *Environ. Modell. Softw.* **2014**, *62*, 437–453. [[CrossRef](#)]
8. Chen, P.; Haboudane, D.; Tremblay, N.; Wang, J.; Vigneault, P.; Li, B. New spectral indicator assessing the efficiency of crop nitrogen treatment in corn and wheat. *Remote Sens. Environ.* **2010**, *114*, 1987–1997. [[CrossRef](#)]
9. Naito, H.; Ogawa, S.; Valecia, M.O.; Mohri, H.; Urano, Y.; Hosoi, F.; Shimizu, Y.; Chavez, A.L.; Ishitani, M.; Selvaraj, M.G.; et al. Estimating rice yield related traits and quantitative trait loci analysis under different nitrogen treatments using a simple tower-based field phenotyping system with modified single-lens reflex cameras. *ISPRS J. Photogramm.* **2017**, *125*, 50–62. [[CrossRef](#)]
10. Rumpler, M.; Daftry, S.; Tscharf, A.; Pretenthaler, R.; Hoppe, C.; Mayer, G.; Bischof, H. Automated end-to-end workflow for precise and geo-accurate reconstructions using fiducial markers. *ISPRS Ann. Photogramm. Remote Sens. Spat. Inf. Sci.* **2014**, *II-3*, 135–142. [[CrossRef](#)]
11. Wang, J.; Badenhorst, P.; Phelan, A.; Pembleton, L.; Shi, F.; Cogan, N.; Spangenberg, G.; Smith, K. Using sensors and unmanned aircraft systems for high-throughput phenotyping of biomass in perennial ryegrass breeding trials. *Front. Plant Sci.* **2019**, *10*, 1381. [[CrossRef](#)] [[PubMed](#)]

12. Niu, Y.; Zhang, L.; Zhang, H.; Han, W.; Peng, X. Estimating above-ground biomass of maize using features derived from UAV-based RGB imagery. *Remote Sens.* **2019**, *11*, 1261. [[CrossRef](#)]
13. Li, G.; Xie, Z.; Jiang, X.; Lu, D.; Chen, E. Integration of Ziyuan-3 multispectral and stereo data for modeling aboveground biomass of Larch Plantations in north China. *Remote Sens.* **2019**, *11*, 2328. [[CrossRef](#)]
14. Hunt, E.R.; Cavigelli, M.; Cst, D.; Mcmurtrey, J.I.; Walthall, C.L. Evaluation of digital photography from model aircraft for remote sensing of crop biomass and nitrogen status. *Precis. Agric.* **2005**, *6*, 359–378. [[CrossRef](#)]
15. Yue, J.; Yang, G.; Tian, Q.; Feng, H.; Xu, K.; Zhou, C. Estimate of winter-wheat above-ground biomass based on UAV ultrahigh-ground-resolution image textures and vegetation indices. *ISPRS J. Photogramm.* **2019**, *150*, 226–244. [[CrossRef](#)]
16. Aasen, H.; Burkart, A.; Andreas, B.; Bareth, G. Generating 3D hyperspectral information with light weight UAV snapshot cameras for vegetation monitoring: From camera calibration to quality assurance. *ISPRS J. Photogramm.* **2015**, *108*, 245–259. [[CrossRef](#)]
17. Li, W.; Niu, Z.; Chen, H.; Li, D.; Wu, M.; Zhao, W. Remote estimation of canopy height and aboveground biomass of maize using high-resolution stereo images from a low-cost unmanned aerial vehicle system. *Ecol. Indic.* **2016**, *67*, 637–648. [[CrossRef](#)]
18. Bendig, J.; Bolten, A.; Bennertz, S.; Broscheit, J.; Eichfuss, S.; Bareth, G. Estimating biomass of barley using crop surface models (CSMs) derived from UAV-based RGB imaging. *Remote Sens.* **2014**, *6*, 10395–10412. [[CrossRef](#)]
19. Zheng, H.; Cheng, T.; Zhou, M.; Li, D.; Yao, X.; Tian, Y.; Cao, W.; Zhu, Y. Improved estimation of rice aboveground biomass combining textural and spectral analysis of UAV imagery. *Precis. Agric.* **2019**, *20*, 611–629. [[CrossRef](#)]
20. Lu, D.; Batistella, M. Exploring TM image texture and its relationships with biomass estimation in Rondônia, Brazilian Amazon. *Acta Amazon.* **2005**, *35*, 249–257. [[CrossRef](#)]
21. Sarker, L.R.; Nichol, J.E. Improved forest biomass estimates using ALOS AVNIR-2 texture indices. *Remote Sens. Environ.* **2011**, *115*, 968–977. [[CrossRef](#)]
22. Kelsey, K.; Neff, J. Estimates of aboveground biomass from texture analysis of Landsat imagery. *Remote Sens.* **2014**, *6*, 6407–6422. [[CrossRef](#)]
23. Jung, J.; Maeda, M.; Chang, A.; Juan, L.; Yeom, J.; McGinty, J. Unmanned aerial system assisted framework for the selection of high yielding cotton genotypes. *Comput. Electron. Agric.* **2018**, *152*, 74–81. [[CrossRef](#)]
24. Chen, Z.; Tao, Z.; Khan, A.; Tan, D.K.Y.; Luo, H. Biomass accumulation, photosynthetic traits and root development of cotton as affected by irrigation and nitrogen fertilization. *Front. Plant Sci.* **2018**, *9*, 173. [[CrossRef](#)]
25. Yang, G.; Tang, H.; Nie, Y. Responses of cotton growth, yield, and biomass to nitrogen split application ratio. *Eur. J. Agron.* **2011**, *35*, 164–170. [[CrossRef](#)]
26. Mariotto, I.; Thenkabail, P.S.; Huete, A.; Slonecker, E.T.; Platonov, A. Hyperspectral versus multispectral crop-productivity modeling and type discrimination for the HypSPIRI mission. *Remote Sens. Environ.* **2013**, *139*, 291–305. [[CrossRef](#)]
27. Zhao, D.L.; Reddy, K.R.; Kakani, V.G.; Read, J.J.; Koti, S. Canopy reflectance in cotton for growth assessment and lint yield prediction. *Eur. J. Agron.* **2007**, *26*, 335–344. [[CrossRef](#)]
28. Olson, D.; Chatterjee, A.; Franzen, D.W.; Day, S.S. Relationship of drone-based vegetation indices with corn and sugarbeet yields. *Agron. J.* **2019**, *11*, 2545–2557. [[CrossRef](#)]
29. Haralick, R.M.; Shanmugam, K.; Dinstein, I. Textural features for image classification. *IEEE Trans. Syst. Man. Cybern.* **1973**, *SMC-3*, 610–621. [[CrossRef](#)]
30. Feng, P.; Wang, B.; Liu, D.; Waters, C.; Xiao, D.; Shi, L.; Yu, Q. Dynamic wheat yield forecasts are improved by a hybrid approach using a biophysical model and machine learning technique. *Agric. For. Meteorol.* **2020**, *285–286*, 107922. [[CrossRef](#)]
31. Rouse, J.W.; Haas, R.H.; Schell, J.A.; Deering, D.W.; Harlan, J.C. *Monitoring the Vernal Advancement of Retrogradation (Green Wave Effect) of Natural Vegetation*; Type III, Final Report; NASA/GSFC: Greenbelt, MD, USA, 1974; pp. 1–371.
32. Gitelson, A.A. Wide dynamic range vegetation index for remote quantification of biophysical characteristics of vegetation. *J. Plant Physiol.* **2004**, *161*, 165–173. [[CrossRef](#)] [[PubMed](#)]

33. Qi, J.; Chehbouni, A.; Huete, A.R.; Kerr, Y.H.; Sorooshian, S. A modified soil adjusted vegetation index. *Remote Sens. Environ.* **1994**, *48*, 119–126. [[CrossRef](#)]
34. Rondeaux, G.; Steven, M.; Baret, F. Optimization of Soil-Adjusted vegetation indices. *Remote Sens. Environ.* **1996**, *55*, 95–107. [[CrossRef](#)]
35. Huete, A.; Justice, C.; Liu, H. Development of vegetation and soil indices for MODIS. *Remote Sens. Environ.* **1994**, *49*, 224–234. [[CrossRef](#)]
36. Broge, N.H.; Leblanc, E. Comparing prediction power and stability of broadband and hyperspectral vegetation indices for estimation of green leaf area index and canopy chlorophyll density. *Remote Sens. Environ.* **2001**, *76*, 156–172. [[CrossRef](#)]
37. Haboudane, D.; Miller, J.R.; Pattey, E.; Zarco-Tejada, P.J.; Strachan, I.B. Hyperspectral vegetation indices and novel algorithms for predicting green LAI of crop canopies: Modeling and validation in the context of precision agriculture. *Remote Sens. Environ.* **2004**, *90*, 337–352. [[CrossRef](#)]
38. Pearson, R.L.; Miller, L.D. *Remote Mapping of Standing Crop Biomass for Estimation of the Productivity of the Short-Grass Prairie, Pawnee National Grasslands, Colorado*; ERIM: Ann Arbor, MI, USA, 1972.
39. Fitzgerald, G.J.; Rodriguez, D.; Christensen, L.K.; Belford, R.; Sadras, V.O.; Clarke, T.R. Spectral and thermal sensing for nitrogen and water status in rainfed and irrigated wheat environments. *Precis. Agric.* **2006**, *7*, 233–248. [[CrossRef](#)]
40. Mohanaiah, P.; Sathyanarayana, P.; GuruKumar, L. Image texture feature extraction using GLCM approach. *Int. J. Sci. Res.* **2013**, *3*, 1–5.
41. Chen, P.; Tremblay, N.; Wang, J.; Vigneault, P.; Huang, W.; Li, B. New index for crop canopy fresh biomass estimation. *Spectrosc. Spect. Anal.* **2010**, *30*, 512–517. (In Chinese with English abstract)
42. Kaizer, H. *A Quantification of Textures on Aerial Photographs*; Technical Report, Tech. Note 121, AD 69484; Boston University Research laboratories: Boston, MA, USA, 1955.
43. Eckert, S. Improved forest biomass and carbon estimations using texture measures from WorldView-2 satellite data. *Remote Sens.* **2012**, *4*, 810–829. [[CrossRef](#)]

Publisher’s Note: MDPI stays neutral with regard to jurisdictional claims in published maps and institutional affiliations.



© 2020 by the authors. Licensee MDPI, Basel, Switzerland. This article is an open access article distributed under the terms and conditions of the Creative Commons Attribution (CC BY) license (<http://creativecommons.org/licenses/by/4.0/>).